

Energy Reconstruction of Non-fiducial Electron-Positron Events in the DAMPE Experiment Using Convolutional Neural Networks

Enzo Putti-Garcia,^{a,1} Andrii Tykhonov,^a Andrii Kotenko,^a Hugo Boutin,^a Manbing Li,^a
Paul Coppin,^a Andrea Serpolla,^a Jennifer Maria Frieden,^b Chiara Perrina,^b Xin Wu^a

^a*Department of Nuclear and Particle Physics, University of Geneva, rue du Général-Dufour 24, CH-1211
Geneva, Switzerland*

^b*Institute of Physics, Ecole Polytechnique Fédérale de Lausanne (EPFL), CH-1015, Lausanne, Switzerland*

E-mail: enzo.putti-garcia@unige.ch

ABSTRACT: The Dark Matter Particle Explorer (DAMPE) is a space-based Cosmic-Ray (CR) observatory with the aim, among others, to study Cosmic-Ray Electrons (CREs) up to 10 TeV. Due to the low CRE rate at multi-TeV energies, we aim to increasing the acceptance by selecting events outside the fiducial volume. The complex topology of non-fiducial events requires the development of a novel energy reconstruction method. We propose the usage of Convolutional Neural Networks for a regression task to recover an accurate estimation of the initial energy.

KEYWORDS: Particle identification methods, Data analysis, Particle detectors

ARXIV EPRINT: [Not yet arxiv number](#)

¹Corresponding author.

Contents

1	Introduction	1
2	Non-fiducial Events	3
3	Classical Energy Reconstruction of Non-fiducial events	3
4	Convolutional method to correct the reconstructed energy	6
5	Results	8
6	Flight data comparison	13
7	Conclusion	13

1 Introduction

The Dark Matter Particle Explorer (DAMPE) is a Cosmic-Ray (CRs) and Gamma-Ray space-based observatory that was launched in 2015 [1]. The main goal of DAMPE is to investigate Cosmic-Ray Electrons plus Positrons¹ (CREs) and Gamma-Rays up to 10 TeV; protons and heavier ions up to a few hundred TeV. The experiment is composed of 4 sub-detectors: a plastic scintillator (PSD) allowing the measurement of the charge[2]; a silicon-tungsten tracker-converter (STK) for precise measurement of the charge, track reconstruction and photon conversion [3]; a bismuth germanium oxide (BGO) calorimeter [4] and a neutron detector (NUD) [5] (Figure 1). These sub-detectors

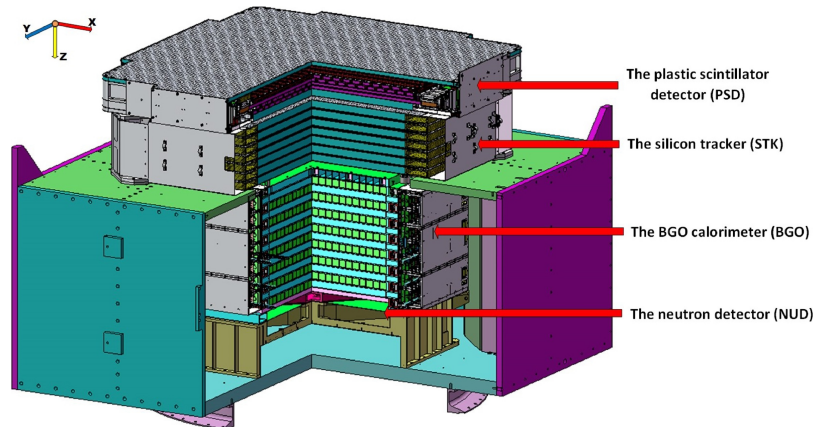


Figure 1: Schematic view of DAMPE. It is composed of a plastic scintillator detector (PSD), a silicon–tungsten track (STK), a BGO calorimeter (BGO), and a neutron detector (NUD) [1].

¹We will refer by electrons to electrons and positrons

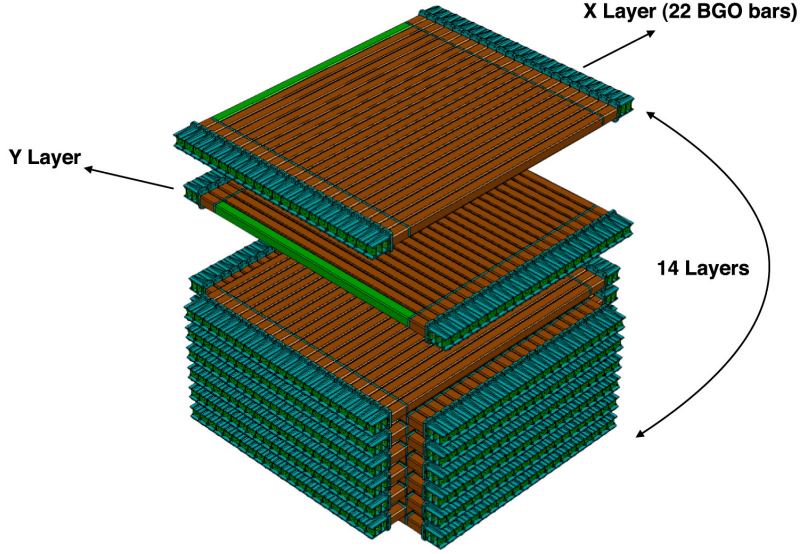


Figure 2: View of the BGO-crystal bar arrangement in the calorimeter. There are 14 layers in a hodoscopic arrangement, each is composed of 22 bars [4].

enable precise measurement of the absolute charge, energy and direction. The calorimeter is composed of 14 layers, each layer containing 22 BGO crystal bars, as shown in Figure 2, with an individual size of $25 \times 25 \times 600 \text{ mm}^3$.

At high energies, CREs undergo energy losses during propagation due to their low mass, primarily from processes such as synchrotron radiation and inverse Compton scattering [6]. Consequently, it is anticipated that electrons at energies higher than a few TeV originate from nearby sources, i.e. within a distance of about one kiloparsec, not older than about 10^5 years [7, 8]. In addition, the aforementioned energy losses lead to a steeper energy spectrum which, resulting on a lower CRE flux with respect to other species, make them relatively rare at high energies. Moreover, several dark matter models predict the emission of electrons and positrons as a result of annihilation or decay [9–11], which could then be seen as e.g. an excess in the high energy CRE spectrum [12]. In 2017, DAMPE published its first measurement of the CRE flux using 1.5 years of data and featuring the direct detection of a break at 0.9 TeV [13]. The energy reach of this measurement was limited to 5 TeV due to the low CRE flux (only 11 events were detected between 3 and 5 TeV). In order to enhance and expand our current understanding in the multi-TeV range, it is essential to increase the statistics and improve the accuracy. Hence, we enlarge the acceptance by selecting events outside of the fiducial volume, that we will call non-fiducial events, which are typically events with a large incidence angle. Since such events are less contained, a non-negligible fraction of their shower will develop outside of the detector. Consequently, the current energy reconstruction methods [1, 14], which are typically applied to events nearly perpendicular to the detector, become less efficient at accurately determining the particle’s energy.

In this paper we propose a new method using Convolutional Neural Networks (CNNs) for the energy reconstruction of electrons on the DAMPE experiment. In section 2, we introduce the concept of non-fiducial events. Section 3 presents the classical method and the reasoning for transitioning to a neural network-based approach. Section 4 showcases the CNN model and training.

In section 5, we present the results and compared the performances of this methods with the classical one. Additionally, we demonstrate how the CNNs enables to avoid the spectral unfolding. In section 6, we show the application of the CNN to data and compare it to Monte-Carlo (MC) simulations. Finally, in section 7 we summarize the findings and contributions of this work.

2 Non-fiducial Events

To motivate the cuts of the non-fiducial event selection, we start by describing the default fiducial selection used in previous publications [13, 15]. We start by following a set of initial selections based on the shower development in the calorimeter, defined as follows:

- Rejecting events that enter the calorimeter from the sides, by imposing a energy fraction in one layer to not exceed 35%.
- Rejecting events where the shower direction cannot be reconstructed.
- Ensuring that the reconstructed shower direction extrapolates to the top and bottom of the BGO sensitive volume, within a distance of 280 mm from the centre, in either the X or Y direction.

These cuts aim to select events that are well reconstructed and contained in the calorimeter. We define non-fiducial events (Figure 3) by inverting the last cut, i.e. by requiring that the top or bottom extrapolation of the shower is not within a distance of 280 mm from the centre.

On top of that, the analysis chain involves standard preselection cuts to reject ions, obvious protons, or poorly reconstructed events in a similar fashion to the 2017 analysis [13].

3 Classical Energy Reconstruction of Non-fiducial events

The standard method for inferring particle energy [14] relies on the total energy deposition in the calorimeter. However, this technique was primarily developed for fiducial events, which are typically associated with low incidence angles. When applied to non-fiducial events, the performance degrades because the shower development occurs largely in the dead material, such as the carbon-fibres and rubbers used as the support structure, and outside the calorimeter, leading to poorer reconstruction and missing energy.

As illustrated in Figure 3, non-fiducial events often have complex shower topologies. This complexity requires the use of more sophisticated techniques for accurate energy reconstruction. Classical methods relied on the deposited energy in each BGO bar, which was obtained from the multi-dynode readout. These techniques enable reconstructing energies up to 10 TeV with a resolution of 1.2% at energies above 100 GeV for electrons/positrons [1]. Generally, the reconstructed energy will be lower than the true energy due to losses in the dead material region between the bars as well as the adjacent bars and the front of the full detector. The work in [14] developed a method to correct for the missing energy. Nevertheless, both methods were optimized for fiducial electrons, for which the lateral and longitudinal shower development is well understood. To evaluate

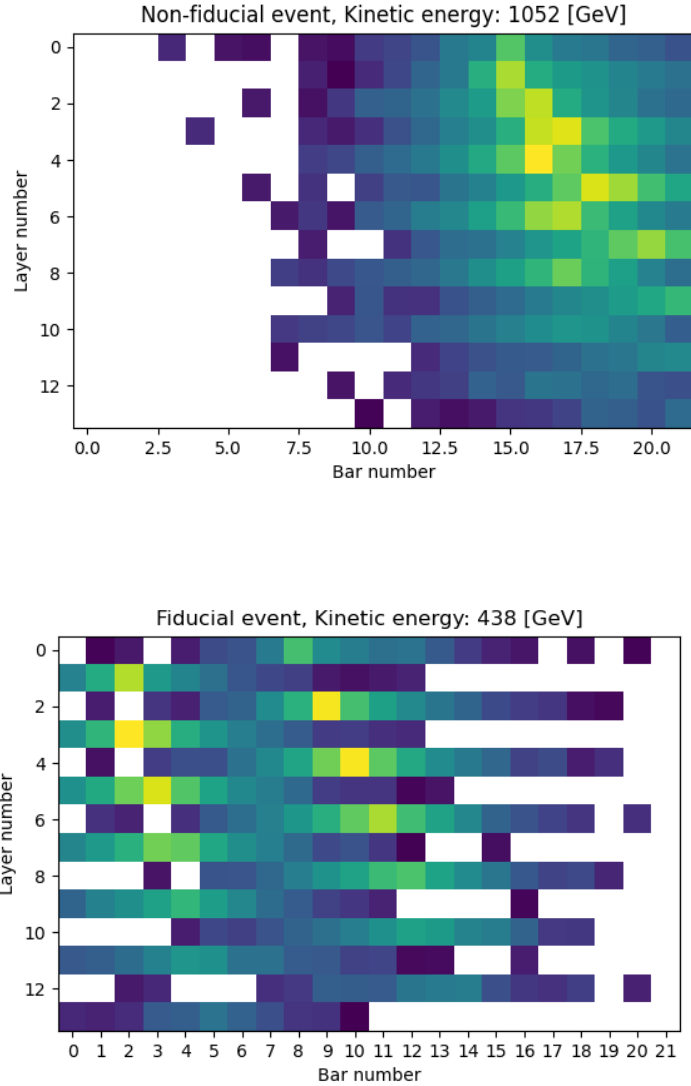


Figure 3: View of a non-fiducial event (top figure) and fiducial event (bottom figure) crossing the calorimeter. The BGO images combine the X-Z and Y-Z views

the efficiency of various reconstruction methods, we compare them by examining the relative error, defined by:

$$r = 1 - \frac{E}{E_{\text{kin}}}, \quad (3.1)$$

where E is the reconstructed energy and E_{kin} is the initial energy of the particle.

In Figure 4, we show the comparisons of methods from [1] and [14]. As can be seen, the energy reconstructed with classical methods E_{rec} is systematically underestimated by at least 5% compared to the kinetic energy. As mentioned earlier, this is expected due to shower leakage and

energy losses in the dead material. However, the corrected energy evaluation, E_{corr} , developed in [14], accounts for those effects.

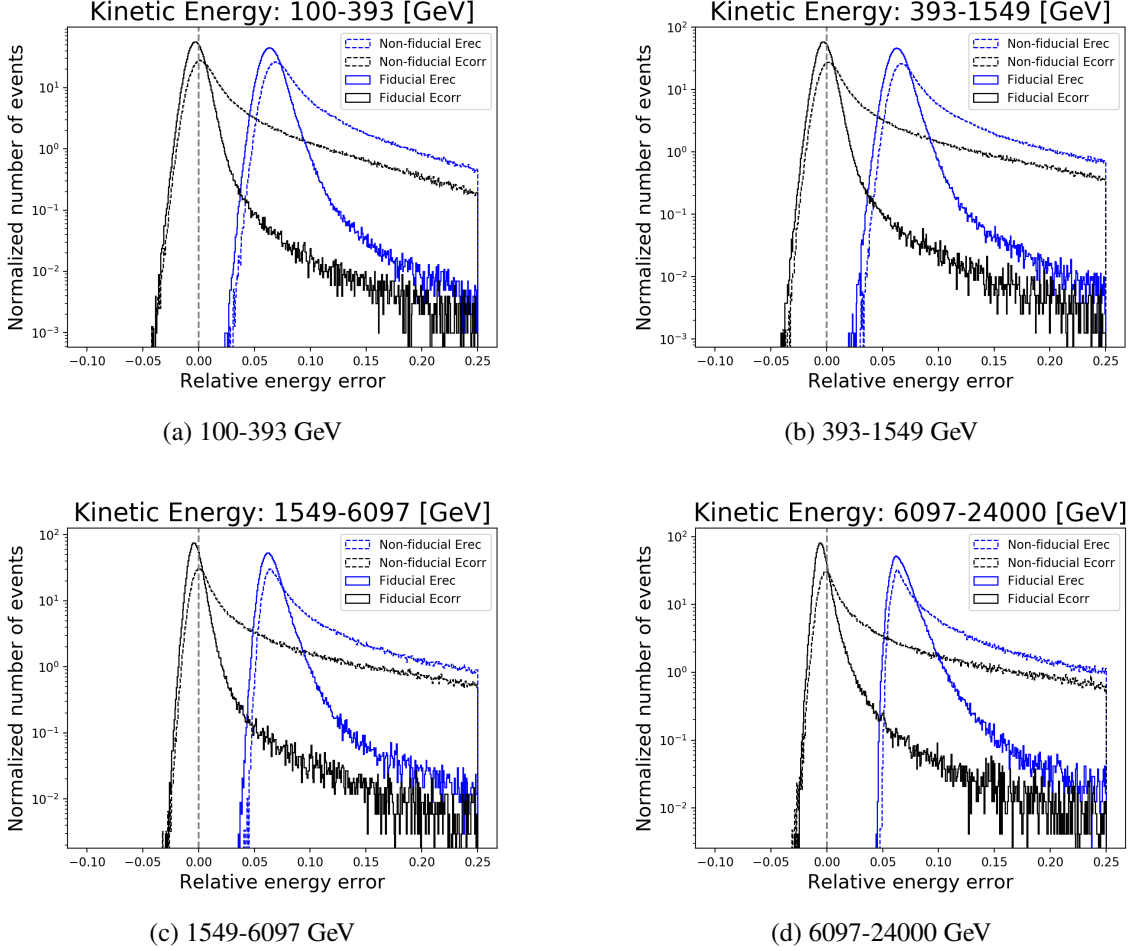


Figure 4: Distribution of the relative energy error obtained with electron MC simulations in four different energy bins, ranging from 100 GeV to 24 TeV. Two types of MC samples are used – fiducial and non-fiducial, analysed with two energy reconstruction methods – standard [1] and corrected [14]. Distributions are denoted as follows: fiducial standard (blue full line), non-fiducial standard (blue dashed line), fiducial corrected (black full line) and non-fiducial corrected (black dashed line). The grey line indicates ideal case when reconstructed energy equals the true kinetic energy.

The corrected method (E_{corr}) [14] provides a better estimation of the true particle energy, as the bulk of the distribution has an estimated energy closer to the kinetic energy, as shown in Figures 4 and 5. However, there is a pronounced tail towards the positive error values, similar to the one of E_{rec} , which is due to events with large energy leakage that cannot be well contained by the calorimeter. On top of that, the energy resolution for both methods becomes worse with increasing energy, as shown in Figure 6.

Overall, we observe that E_{corr} is optimized for fiducial events. To correct the energy of non-fiducial events, a new method is required. It is developed in this paper using CNNs approach, where

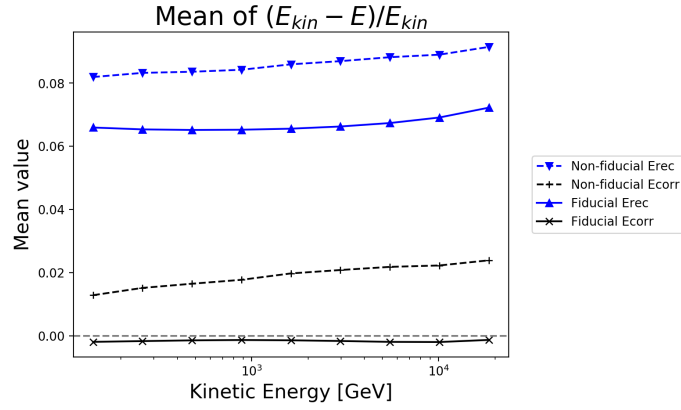


Figure 5: Mean of the relative energy error as a function of kinetic energy for the different energy reconstruction methods.

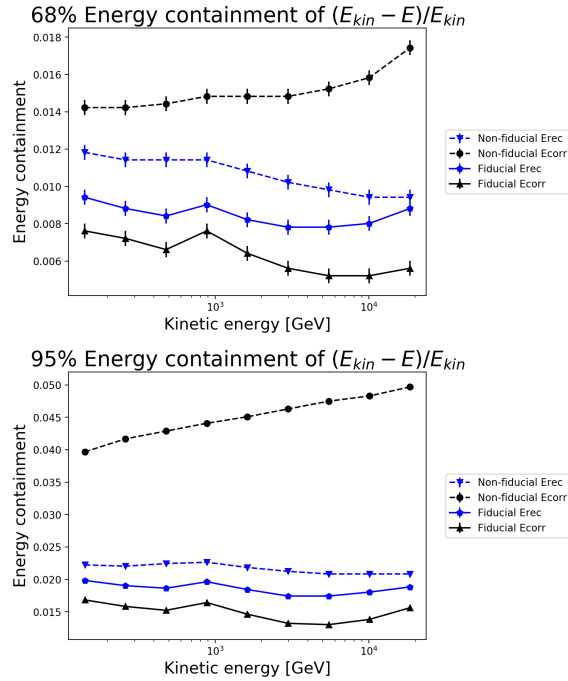


Figure 6: Energy resolution as a function of kinetic energy. Top plot: 68% containment, bottom plot: 95% containment.

a neural network is train to predict the relative error of the true energy and the reconstructed energy. The CNN will be presented in the next section, where we will also evaluate its accuracy.

4 Convolutional method to correct the reconstructed energy

Machine Learning (ML) techniques have been widely applied in various domains of physics [16]. The DAMPE collaboration has utilized such techniques for tasks ranging from the discrimination

between protons and electrons [15, 17], to track reconstruction [18], and calorimeter saturation correction [19].

To accurately recover the true kinetic energy of non-fiducial events, we train a CNN to perform a regression of the relative error between the reconstructed energy (E_{rec}) and the true energy of the particle (E_{kin}), defined by:

$$r = 1 - \frac{E_{\text{rec}}}{E_{\text{kin}}}. \quad (4.1)$$

We chose to use the relative error instead of the true kinetic energy because it allows the model to achieve better performances, as the values of r are bounded between 0 and 1. The goal is to obtain a prediction for the ratio that will then be used to correct the energy. As an input to the CNN we use an image of the BGO calorimeter, combining the X-Z and Y-Z views, as illustrated in Figure 3. Since the layers of the calorimeter are placed in a hodoscopic arrangement, this results in a correlation between both views. As a result, we expect that training a CNN with each view separately would result in a poorer resolution, as discussed in [18, 19] since both views are correlated. The input to the CNN is normalise by the maximum deposited energy in the calorimeter resulting in images with pixel values between 0 and 1.

The model was trained based on MC simulations of electrons. The training was done based on Monte-Carlo (MC) simulations, generated using Geant4 (version 10.05) [20] with FTFP-BERT physics. The simulation samples are weighted following a E^{-3} power law. The MC samples were processed following the selection procedure described in section 2. We divide MC into a training sample and a validation sample by selecting 70% of the full MC sample for the training and the remaining 30% as validation sample. To be able to have an uniform performance over all energies, we split the sample into 10 bins equally spaced in logarithm of kinetic energy (from 100 GeV to 24 TeV), then choose the energy bin with the lowest number of events and select the same number of events in each of the other energy bins. The resulting training sample was composed of 1'084'912 events.

We used Tensorflow 2 [21] as the framework for training of the CNN. The model structure is the following one:

The activation function used is a Rectified Linear Unit (ReLU). The different convolutional layers are use with a kernel size of 3×3 . Finally, as a loss function to evaluate whether the CNN training goes under- or over- fitting we look at the evolution of the mean squared error as a function of the epochs, defined by:

$$\frac{1}{m} \sum_{i=0}^m (\hat{r}_i - r_i)^2, \quad (4.2)$$

where m is the number of training samples, r_i is the relative error between E_{rec} and E_{kin} as defined in Equation 4.1, and \hat{r}_i is the CNN prediction.

Figure 8 shows the convergence of the training and validation sample after 40 epochs. As we can see the loss has converged close to $1.75 \cdot 10^{-4}$ ($1.50 \cdot 10^{-4}$ for the validation loss). While the loss for the validation sample has greater oscillations, this can be explained by the fact that its composition is different at all energies, meaning that there is no balance between low energy and high energy.

CNN Architecture Diagram

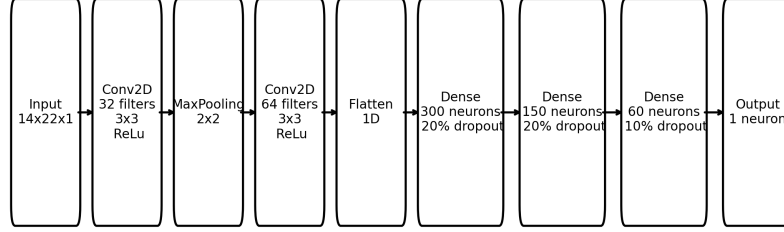


Figure 7: CNN model structure.

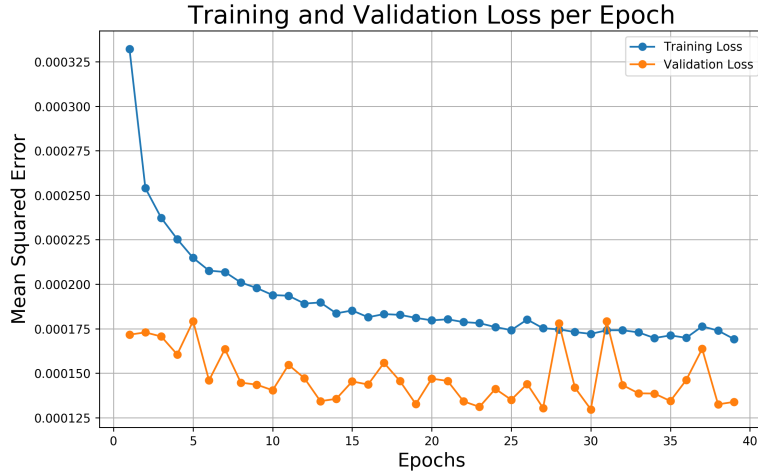


Figure 8: Evolution of the loss, defined as the mean squared error for the training sample (blue curve) and validation sample (orange curve).

5 Results

The energy output is obtained from the CNN output, according to Equation 4.1, as follows:

$$E_{\text{CNN}} = \frac{E_{\text{rec}}}{1 - r}, \quad (5.1)$$

To estimate the CNN’s efficiency and compare it to the classical methods (see Figure 4), we

also calculate the relative error for E_{CNN} , defined by:

$$r_{\text{CNN}} = 1 - \frac{E_{\text{CNN}}}{E_{\text{kin}}}. \quad (5.2)$$

In Figure 9, we compare the reconstructed energy obtained by the classical methods (blue curve and yellow curve) [14] and the CNN (green curve) for electron MC. While the CNN was trained on electrons only, its performance is expected to be identical for both electrons and positrons since their electromagnetic showers are effectively indistinguishable at energies at energies sufficiently higher than 10 MeV (see Figure 34.11 from [22, page 582]).

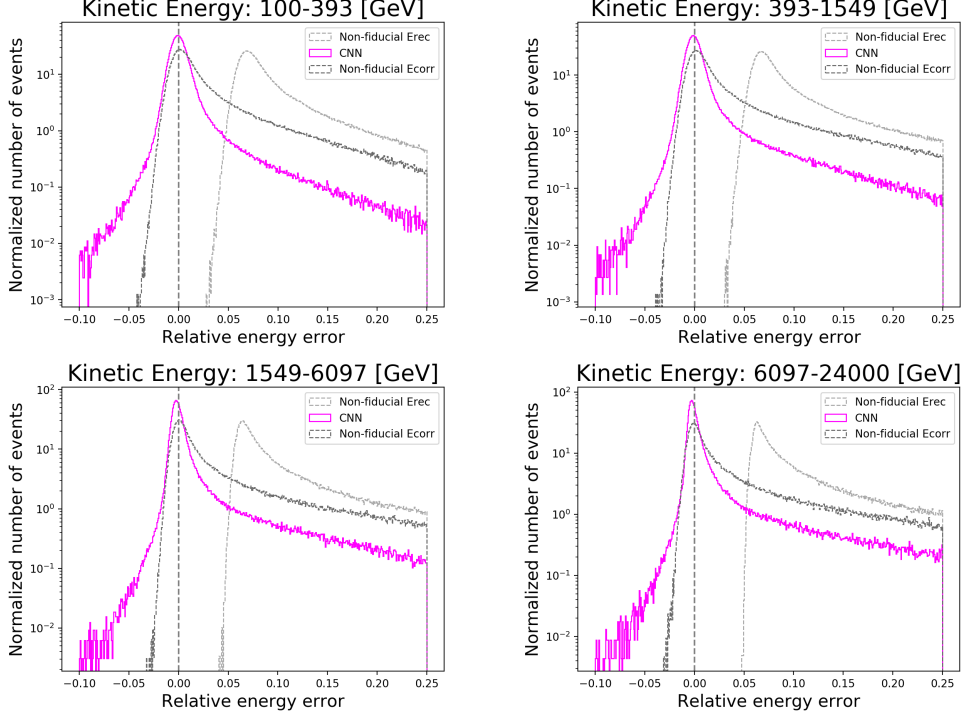


Figure 9: The distribution of the relative energy error (Equation 4.1) for electron MC samples ranging from 100 GeV to 24 TeV. Light grey curve: for the standard energy reconstruction method [1], dark grey curve: standard electron energy correction method [14] and magenta curve: CNN method. Grey vertical line indicates ideal case when reconstructed energy equals the true kinetic energy.

From Figure 9, we can see that the relative energy reconstruction error of the CNN model (E_{CNN}) has a distribution centred close to 0, similar to E_{corr} , indicating an improvement over E_{rec} . Additionally, there is a decrease in the number of events where the energy is underestimated compared to E_{kin} . However, a slight bias toward negative values is observed, leading to a mild overestimation of the initial energy ($E_{\text{CNN}} > E_{\text{kin}}$). To quantify the efficiency of the CNN method with respect to other methods, we analyse the 68%/95% containment values of the distributions in Figure 9, as shown in Figures 10 and 11 respectively. Figure 10 shows that the mean value for the CNN method stays stable at all energy, demonstrating apparent improvement over the E_{corr} method. The same can be seen for 68%/95% containments in Figure 11. In particular, the 68%

containment for the CNN method is consistently lower (better) than for the standard methods and decreases (improves) with energy. The 95% containment shows similar behaviour although with less improvement compared to the standard methods, especially at high energies. These results demonstrate a significant improvement compared to the classical methods.

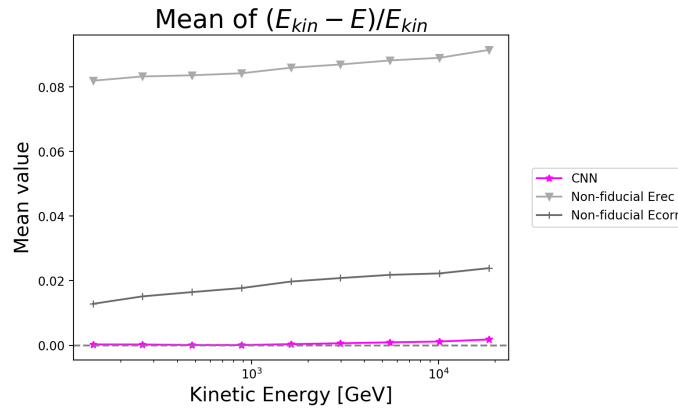


Figure 10: Plot of the mean of the relative energy error (Equation 4.1) for electron MC samples ranging from 100 GeV to 24 TeV. Light grey curve: for the standard energy reconstruction method [1], dark grey curve: standard electron energy correction method [14] and magenta curve: CNN method. Horizontal grey line indicates ideal case when reconstructed energy equals the true kinetic energy.

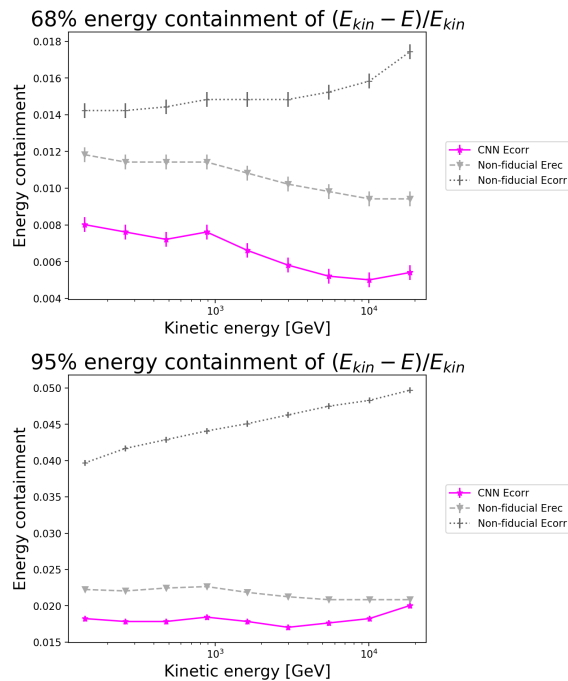


Figure 11: The 68% and 95% containment of the relative energy reconstruction errors as function of the kinetic energy.

As we have shown, the CNN method allows to recover the missing shower energy in the calorimeter and consequently to have a close estimation of the real electron energy.

Unfolding [23] is commonly used in the analysis of CR data to estimate the number of events as a function of the true energy by leveraging knowledge from the detector (typically using MC samples). This process involves constructing a response matrix that characterizes the deposited energy as a function of the kinetic energy (Figure 12). We will demonstrate that the developed CNN method eliminates the need for unfolding in flux calculations.

To illustrate this, we will define a response matrix for each energy reconstruction method and use the Python library pyUnfold [24] to apply the unfolding method. We will then compare the obtained flux (after unfolding) to those derived without the unfolding step, showcasing the advantages of the CNN approach.

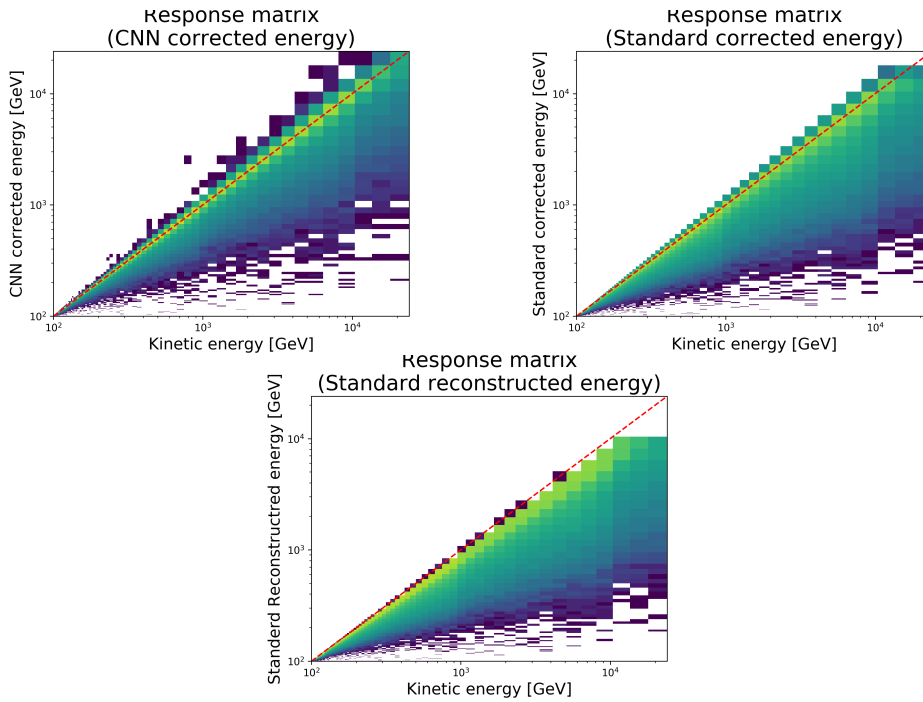


Figure 12: Response matrix of the three energy reconstruction methods: CNN-corrected, standard corrected and standard reconstruction (no correction). Red line indicates a diagonal of a matrix.

We can now compare the normalised number of events before and after unfolding.

From Figure 13, it can be seen that the normalized CNN energy is in good agreement with the kinetic energy, the same can be said for the unfolded CNN energy.

Figure 14 shows the ratio of electron energy spectrum calculated using the CNN-corrected energy method, with and without the unfolding, divided by the truth spectrum defined in the MC simulation. We can see that the unfolding procedure does not improve the electron spectrum estimation compare to case without unfolding. In fact we can see an oscillation. On top of that, the unfolding procedure has an edge effect at low and high energies.

We conclude that the CNN method can recover the real energy of the event accurately and with minimal bias. Because of this, unfolding is not needed to compute the electron flux. This is

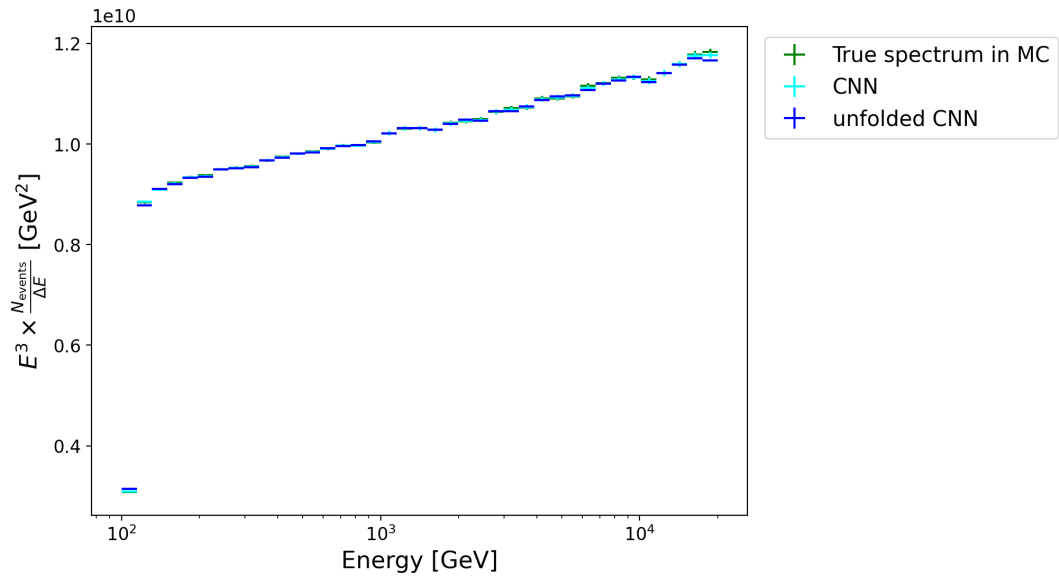


Figure 13: Electron kinetic energy spectrum obtained with the CNN method with and without the unfolding procedure (cyan and blue lines respectively) compared with the truth spectrum defined in MC.

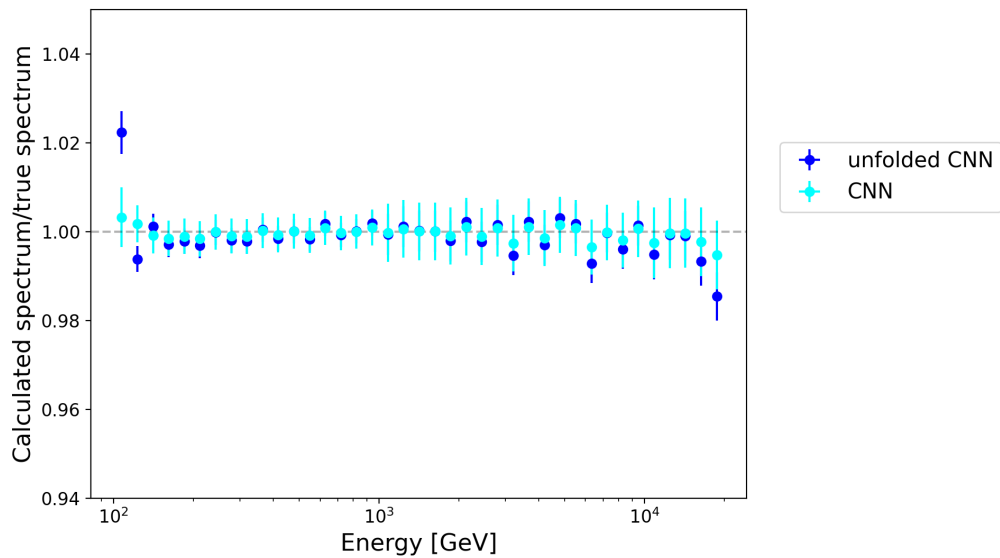


Figure 14: Ratio of the calculate spectrum, with and without unfolding, divided by the truth kinetic energy spectrum defined in MC.

advantageous because it enables avoiding unfolding edge effects.

6 Flight data comparison

In the previous section we looked at the efficiency of the CNN applied to MC and compared it with the classical methods (E_{rec} and E_{corr}). However, to be able to use such technique in future analyses, we need to confirm the previous observations for real data. To do so, we select a sample of events (data and MC) in a narrow energy range using the reconstructed energy since the kinetic energy is not accessible for real data. The electrons in real data are selected with another CNN, trained to separate electrons from protons. The training sample for this CNN was created using electrons and protons MC. Figures 15 and 16 show the output of the classifier for 5 energy samples divided in bins of E_{rec} : 200-205 GeV, 300-305 GeV, 400-410 GeV, 460-500 GeV and 960-1000 GeV², which represents the score values used to select a clean sample. A cut value of 4 is used to select a clean sample. Table 1 shows the number of events that pass this cut. Finally, in Figure 17 we plot for each energy range the distribution of energy reconstructed with the CNN method for both real data and MC as shown.

In Figure 17 we can see an overall adequate agreement between real data and MC showing that the qualitative behaviour of the CNN is similar between data and MC, also shown by the ratio between data and MC. Adjusting the cut value of the CNN classifier to 3 worsens the agreement, while increasing it to 5 improves the match, suggesting that the background fraction plays a role in shaping the distributions shown in Figure 17. Additionally, distinct features are visible in the tails of the distributions. These features arise because, for a given kinetic energy, a particle can deposit only a fraction of its energy, as illustrated by the response matrix in Figures 12. The CNN's ability to more accurately estimate kinetic energy leads to the emergence of additional structures within the tail, corresponding to various kinetic energy values. To have a more quantitative way of showing the comparison between data and MC as shown in Figures 18 and 19, we looked at the mean value and the 68/95 % energy containment of the distributions shown in Figure 17. The comparison between data and MC is performed using two metrics: the mean value and the 68/95% energy containment. The results show a strong agreement in the mean values between data and MC, indicating consistency in the central tendencies. However, the energy containment demonstrates tighter bounds in the MC compared to the real data. Despite this difference, both data and MC exhibit similar overall behaviour, as illustrated in Figures 18 and 19, which validate the alignment of the models in capturing key trends.

7 Conclusion

Studies suggest the potential for the direct observation of cosmic ray electron (CRE) and positron sources at TeV scale [7, 8]. Additionally, various dark matter models predict electron and positron production through annihilation or decay [9], which may manifest as an excess in the high energy CRE spectrum. However, due to their light mass, CREs experience significant energy losses during propagation. Combined with an already lower flux compared to the other particles species, CREs are relatively rare at high energies. To increase statistics and extend DAMPE's current results

²The last two energy bins are larger due to low statistics.

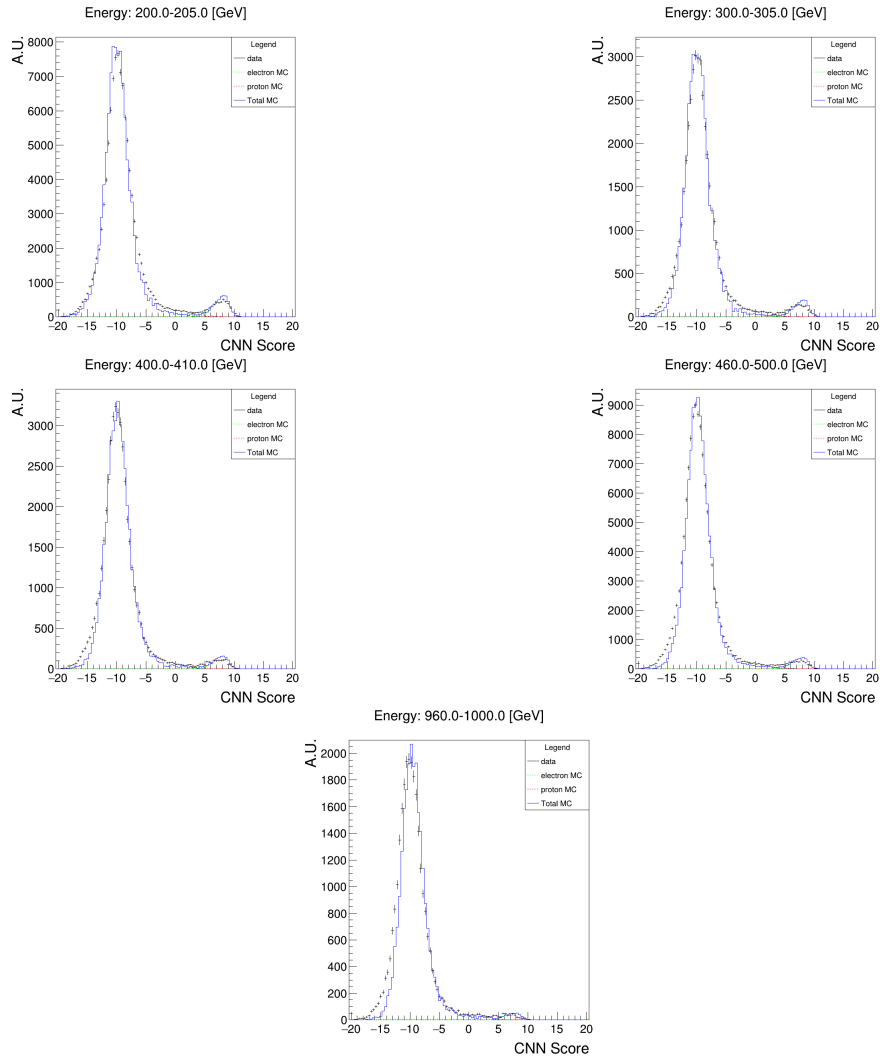


Figure 15: Distribution of CNN classifier for data and MC samples for different energy bins in linear scale.

Table 1: Number of MC and data events passing the CNN classifier, for a cut value of 4. Last column represents the fraction of background that passes the cut.

Energy range [GeV]	proton MC	electron MC	data	background fraction
200-205	279	4763	4793	5.8%
300-305	63	1508	1429	4.4%
400-410	63	1246	1215	4.5 %
460-500	254	3045	2988	8.5 %
960-1000	49	401	434	11.3 %

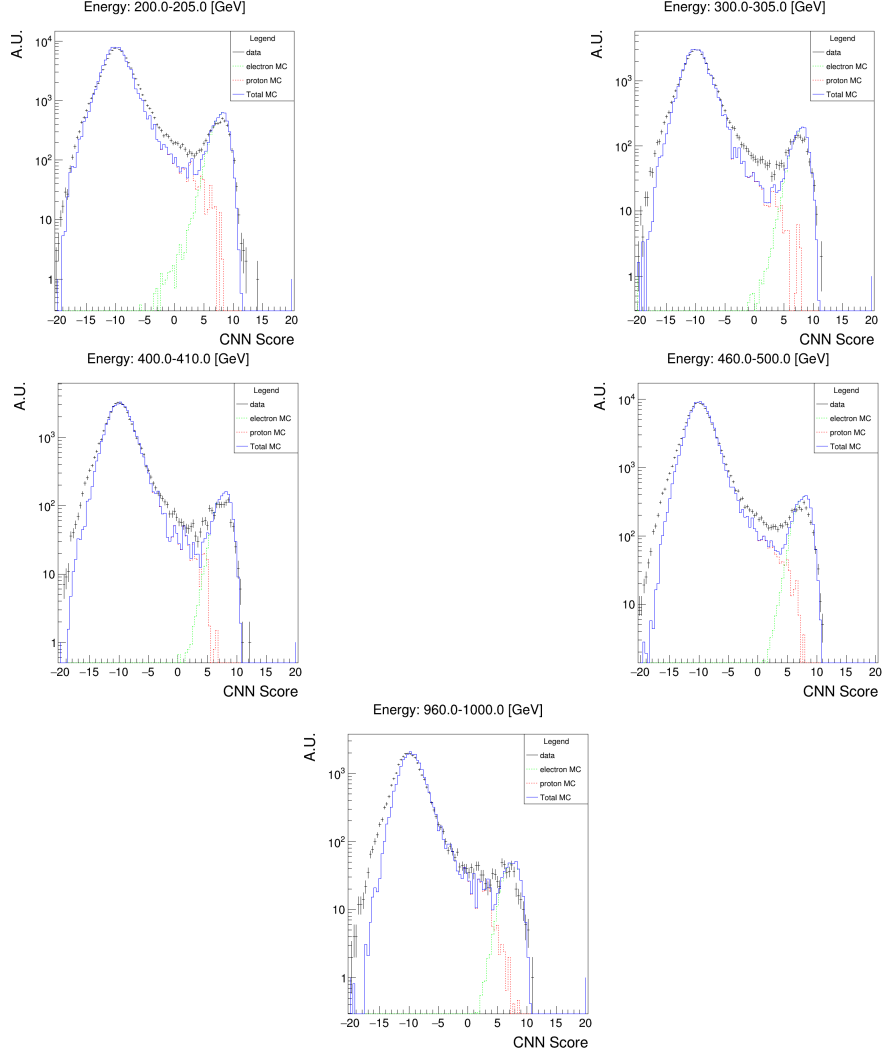


Figure 16: Distribution of CNN classifier for data and MC samples for different energy bins in logarithmic scale.

[13], the inclusion of non-fiducial electrons and positron is necessary. However, incorporating these events introduces challenges due to their complex shower topology in the calorimeter. One such challenge, addressed in this paper, is their accurate energy reconstruction. As demonstrated, classical methods are not well-suited for non-fiducial events (see Figures 4,5,6). Therefore, the application of a Convolutional Neural Network (CNN) for regression offers a promising solution. The training process for the CNN involved splitting the Monte Carlo sample into training (70%) and validation (30%) sets, with input images from the BGO calorimeter. The regression was performed on the relative error between the reconstructed energy and the true kinetic energy. Figure 8 shows the evolution of the CNN's performance, measured via the mean squared error (Equation 4.2). We evaluated the CNN's effectiveness by comparing its performance to classical methods, focusing on the relative error distributions (Figure 9). Additionally, we quantified the CNN's performance. The mean values (Figure 10) have shown stable results at all energies (close to a mean of 0). The

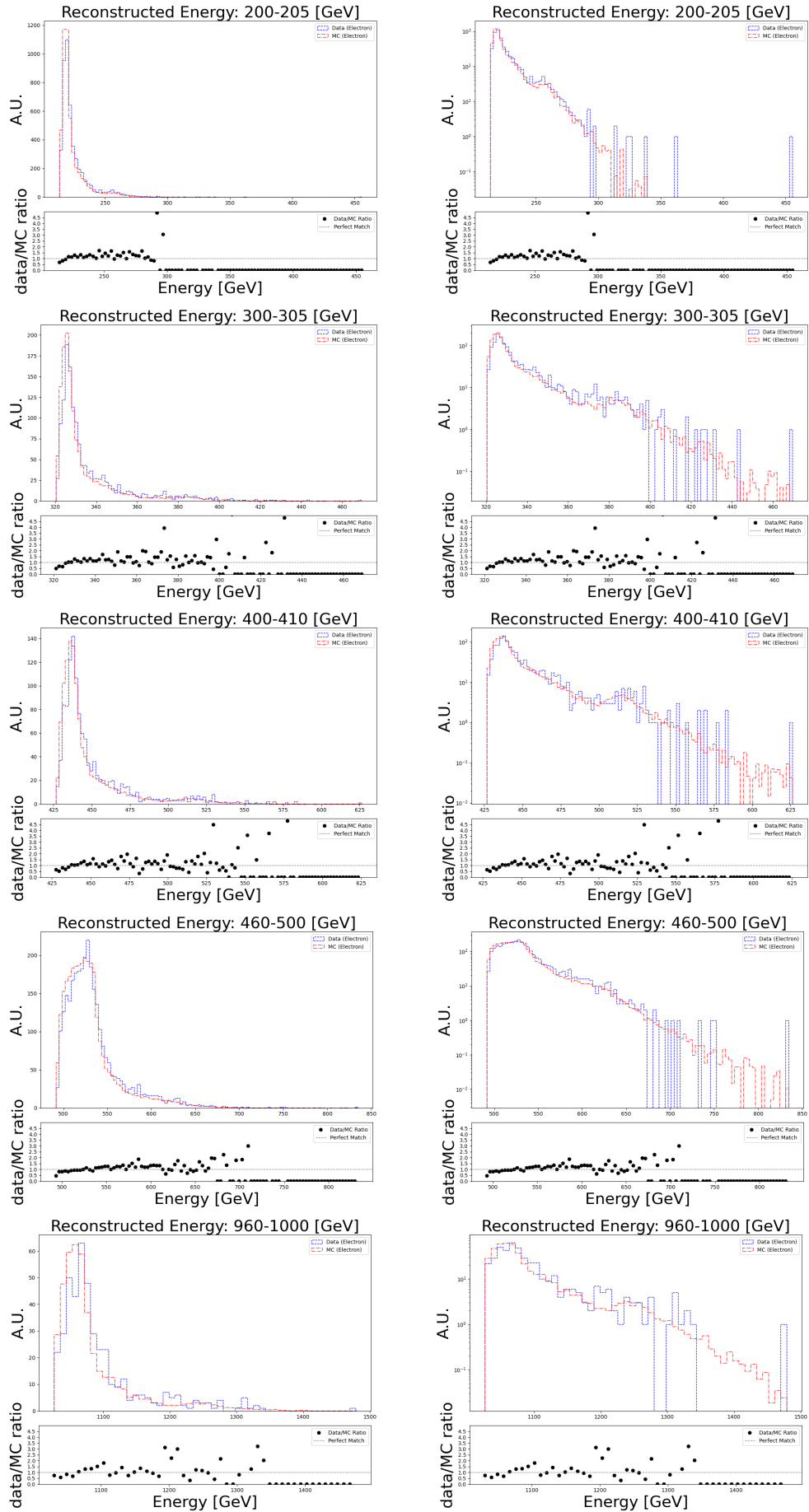


Figure 17: Distribution of CNN energy correction method for data and MC samples. Lower plot are the ratio between real and MC data. Left plots are in linear scale, right plots are in log scale.

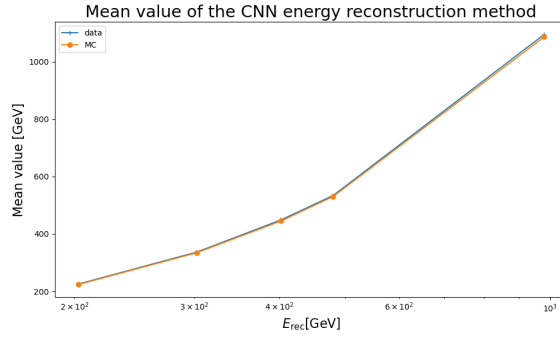


Figure 18: Mean value of the CNN reconstructed energy for data and MC as a function of the standard energy reconstruction method [1].

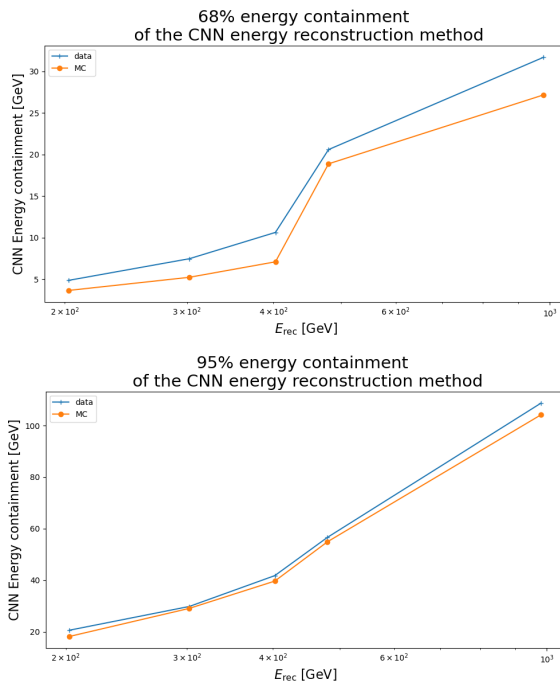


Figure 19: The 68% and 95% containment of the CNN energy reconstruction method as a function of standard energy reconstruction method [1].

68% and 95% energy resolution plots (Figure 11) show an improvement compared to the classical methods. Then, we considered unfolding, a step that is usually performed during a flux analysis, but our results demonstrated that the CNN approach eliminates the need for unfolding, avoiding the introduction of edge effects as shown in Figure 14.

Although MC demonstrates the improvement of the CNN method over the classical approaches, it is essential to validate these results with data. To achieve this, we used an ML classifier, more precisely a CNN, to select a clean sample, from data, of electrons and divided them into five samples based on energy ranges, [200-205, 300-305, 400-410, 460-500, 960-1000] GeV. We then compared it to a MC sample selected using the same criteria. Figure 17 shows good qualitative

agreement between the two, as estimated by the ratio of both distributions. Similar conclusions can be reached by looking at the mean of distributions and the 68/95% energy containment for real data and MC. In conclusion, the CNN method offers a significant improvement in accuracy and precision of estimating/recovering the initial energy.

References

- [1] J. Chang, G. Ambrosi, Q. An, R. Asfandiyarov, P. Azzarello, P. Bernardini et al., *The dark matter particle explorer mission*, *Astroparticle Physics* **95** (2017) 6.
- [2] Y. Yu, Z. Sun, H. Su, Y. Yang, J. Liu, J. Kong et al., *The plastic scintillator detector for dampe*, *Astroparticle Physics* **94** (2017) 1.
- [3] P. Azzarello, G. Ambrosi, R. Asfandiyarov, P. Bernardini, B. Bertucci, A. Bolognini et al., *The dampe silicon–tungsten tracker*, *Nuclear Instruments and Methods in Physics Research Section A: Accelerators, Spectrometers, Detectors and Associated Equipment* **831** (2016) 378.
- [4] Y. Wei, Y. Zhang, Z. Zhang, L. Wu, S. Wen, H. Dai et al., *Performance of the dampe bgo calorimeter on the ion beam test*, *Nuclear Instruments and Methods in Physics Research Section A: Accelerators, Spectrometers, Detectors and Associated Equipment* **922** (2019) 177.
- [5] Y.-Y. Huang, T. Ma, C. Yue, Y. Zhang, M.-S. Cai, J. Chang et al., *Calibration and performance of the neutron detector onboard of the dampe mission*, *Research in Astronomy and Astrophysics* **20** (2020) 153.
- [6] F.C. Jones, *Inverse compton scattering of cosmic-ray electrons*, *Phys. Rev.* **137** (1965) B1306.
- [7] C. Evoli, E. Amato, P. Blasi and R. Aloisio, *Galactic factories of cosmic-ray electrons and positrons*, *Phys. Rev. D* **103** (2021) 083010.
- [8] T. Kobayashi, Y. Komori, K. Yoshida and J. Nishimura, *The Most Likely Sources of High-Energy Cosmic-Ray Electrons in Supernova Remnants*, *apj* **601** (2004) 340.
- [9] M.S. Turner and F. Wilczek, *Positron line radiation as a signature of particle dark matter in the halo*, *Physical Review D* **42** (1990) 1001.
- [10] J. Conrad and O. Reimer, *Indirect dark matter searches in gamma and cosmic rays*, *Nature Physics* **13** (2017) 224.
- [11] AMS COLLABORATION collaboration, *Towards understanding the origin of cosmic-ray positrons*, *Phys. Rev. Lett.* **122** (2019) 041102.
- [12] M. Pohl, *Cosmic-ray electron signatures of dark matter*, *Phys. Rev. D* **79** (2009) 041301.
- [13] DAMPE Collaboration, *Direct detection of a break in the teraelectronvolt cosmic-ray spectrum of electrons and positrons*, *Nature* **552** (2017) 63.
- [14] C. Yue, J. Zang, T. Dong, X. Li, Z. Zhang, S. Zimmer et al., *A parameterized energy correction method for electromagnetic showers in bgo-ecal of dampe*, *Nuclear Instruments and Methods in Physics Research Section A: Accelerators, Spectrometers, Detectors and Associated Equipment* **856** (2017) 11.
- [15] D. Droz, A. Tykhonov, X. Wu, F. Alemanno, G. Ambrosi, E. Catanzani et al., *A neural network classifier for electron identification on the dampe experiment*, *Journal of Instrumentation* **16** (2021) .
- [16] G. Carleo, I. Cirac, K. Cranmer, L. Daudet, M. Schuld, N. Tishby et al., *Machine learning and the physical sciences*, *Reviews of Modern Physics* **91** (2019) 045002.

- [17] Z. Xu, X. Li, M. Cui, C. Yue, W. Jiang, W. Li et al., *An unsupervised machine learning method for electron–proton discrimination of the dampe experiment*, *Universe* **8** (2022) .
- [18] A. Tykhonov, A. Kotenko, P. Coppin, M. Deliyergiyev, D. Droz, J.M. Frieden et al., *A deep learning method for the trajectory reconstruction of cosmic rays with the dampe mission*, *Astroparticle Physics* **146** (2023) 102795.
- [19] M. Stolpovskiy, X. Wu, A. Tykhonov, M. Deliyergiyev, C. Perrina, M.M. Salinas et al., *Machine learning-based method of calorimeter saturation correction for helium flux analysis with dampe experiment*, *Journal of Instrumentation* (2022) .
- [20] S. Agostinelli, J. Allison, K. Amako, J. Apostolakis, H. Araujo, P. Arce et al., *Geant4—a simulation toolkit*, *Nuclear Instruments and Methods in Physics Research Section A: Accelerators, Spectrometers, Detectors and Associated Equipment* **506** (2003) 250.
- [21] M. Abadi, A. Agarwal, P. Barham, E. Brevdo, Z. Chen, C. Citro et al., *TensorFlow: Large-scale machine learning on heterogeneous systems*, 2015.
- [22] PARTICLE DATA GROUP collaboration, *Review of particle physics*, *Phys. Rev. D* **110** (2024) 030001.
- [23] G. D’Agostini, *A multidimensional unfolding method based on bayes’ theorem*, *Nuclear Instruments and Methods in Physics Research Section A: Accelerators, Spectrometers, Detectors and Associated Equipment* **362** (1995) 487.
- [24] J. Bourbeau and Z. Hampel-Arias, *Pyunfold: A python package for iterative unfolding*, *The Journal of Open Source Software* **3** (2018) 741.